07

InP-based Mach-Zender modulator with adjustable extinction coefficient

© S.V. Ishutkin,[1,2] V.S. Arykov,[2] I.V. Yunusov,[2] M.V. Stepanenko,[2] V.S. Smirnov,[1]
P.E. Troyan,[2] Yu.S. Zhidik[2,3]

[1]Research and Production Company „Micran",
634041 Tomsk, Russia
[2]Tomsk State University of Control Systems and Radioelectronics,
634050 Tomsk, Russia
[3]V.E. Zuev Institute of Atmospheric Optics of Siberian Branch RAS,
634055 Tomsk, Russia
e-mail: zhidikyur@mail

Received July 8, 2023
Revised September 13, 2023
Accepted September 14, 2023

Development of the Mach-Zender electrooptic modulator with adjustable extinction coefficient provided by electrical tuning of the input splitter based on multimode interferometer. Electrooptical bandwidth of the modulators was higher than 32 GHz, modulus of electric signal reflectance from the input was not higher than -12 dB within the range up to 43 GHz, half-wave voltage was equal to 2.8 V at 1550 nm. However, electrical tuning of the input splitter extended the extinction ratio of the modulator from the initial 21.5 to 29.5 dB.

Keywords: beam splitter, splitter imbalance, waveguides, amplitude modulation.

DOI: 10.61011/TP.2023.11.57502.172-23

Introduction

Currently, integral optoelectronics is still being an extensively developed area. Photon integrated circuit are widely used for communication networking, high-speed computation, creation of coherent and non-coherent light sources, biophotonics, optical signal processing, etc. Communications market is one of the main drivers of microwave photonics development. Fast global distribution of wireless Internet access wearable technology, development and introduction of 4 G and 5 G mobile networks, video service and IoT expansion increase the network traffic exponentially [1,2]. Traditional electric communication lines have not met the capacity requirements any longer. Transmission of ever increasing amount of data downloaded and transmitted to remote data center servers is the main source of fiber-optic communication link loading. For this, infrastructure built on the appropriate equipment is required.

InP-based Mach-Zender electrooptic modulator (EOM) is one the key microwave photonics components [3–5]. Having the optical wave amplitude control capability, this device converts electrical signals to optical signals for further processing and/or transmission. Modulator's extinction ratio (ER) measures the device capability of optical wave power controlling. ER is mainly limited by power dividing asymmetry in the beam splitter at the modulator input. This is associated with the fact that the equipment manufacturing processes feature reproduction accuracy, so-called manufacturing tolerances, resulting in modulator parameter spread. In mass production, uniformity of devices between batches is more important than the individual parameter values. This defines the device yield ratio and final price. uniformity of device parameters, in turn, depends on the manufacturing process tolerances. Various approached may be used to achieve the uniformity. One of the approaches involves factory modernization to use the equipment that ensures lower tolerances. This allows the problem to be solved, but may be overpriced. Another approach involves expansion of manufacturing tolerances due to fine tuning capability after manufacturing to ensure the use of existing process equipment.

Distributed feedback (DFB) lasers are an example of successful utilization of tunable devices in the integrated optoelectronics. In DB-lasers, the optical output wavelength may be retuned electrically [6–8]. This is implemented by bandwidth fine tuning of the internal Bragg grating filter. Retuning range is usually not too large — $\pm 1-4$ nm, but such approach allows to avoid the need to have lasers intended for a strictly defined wavelength. The variety of devices is simplified and, therefore, their cost is reduced.

A number of studies have presented tunable beam splitters based on multimode interferometers (MMI) [9], both individual and integrated in more complex systems. In [10], a general model for forecasting the division ratio retuning range of beam splitters based on symmetrical and asymmetrical MMI was presented. The authors have demonstrated a 20% retuning range using the symmetrical MMI case (2×2). Another study [11,12] has shown tunable MMI (2×2) splitter design and manufacturing process. The authors have achieved a wide division ratio retuning range from 90:10 to 30:70. Integrated balanced photodetector with tunable MMI (2×2) splitter is described in [13,14] . The tunable splitter enabled power balance to be achieved on the receiver photodiodes. Development of widely-tunable MMI-based (1×1) laser is described in [15] . Laser wavelength tuning capability within 38 nm has been demonstrated experimentally. A space-saving electrooptic modulator model on the basis of a tunable MMI (1×1) has been developed in [16] . The calculation has shown that ER equal to 35 dB may be achieved for the device length of $350\,\mu$m (without considering the electric adsorption effects). A Mach-Zender double parallel modulator design with three MMI splitters, one of which was tunable, was offered in [17].

The objective of the study is to achieve a Mach-Zender electrooptic modulator with dynamic extinction coefficient control function. This will enable fine tuning of modulator extinction ratio after manufacturing , thus, ensuring modulator uniformity. Control is to be implemented through provision of an electrically tunable MMI (1×2) splitter at the modulator input. While usually this is an uncontrolled component and its division ratio is fixed at the modulator's optical waveguide formation stage.

1. Materials and methods

The study used two-inch semi-insulating InP substrates with *p-i-n* InP/InGaAsP heterostructure formed on their surface. *p*- and *n*-regions were formed with a variable alloying profile. *p*-InP-region was Zn-alloyed with a maximum alloying level of $2\cdot10^{18}\,\mathrm{cm}^{-3}$, *n*-InP-region was Si-alloyed with a maximum alloying level of $5\cdot10^{18}\,\mathrm{cm}^{-3}$. In *i*-region of the *p-i-n*-structure, multiple quantum wells (MQW) on the basis of the InP/InGaAsP superlattice were formed. A contact *p*-InGaAs layer was formed above the heterostructure layers in order to form ohmic contacts. The total thickness of the epitaxial layers was about $3.5\,\mu$m (excluding the semi-insulating buffer layer).

Figure 1 shows an electrooptic modulator manufacturing process route. Layer configuration and manufacturing process of the tunable MMI splitter at the modulator input were similar to those for active optical waveguide sections (components with top ohmic Ti/Pt/Au contact in Figure 1). The process route consisted of the following process module sequence:

— formation of dielectric SiN_x mask for further formation of optical waveguide structures;

— first plasma-chemical etching of p-layers of the heterostructure on the dielectric mask;

— removal of a part of dielectric mask from passive components of the electrooptical path;

— second plasma-chemical etching of *p*- and*i*-layers of the heterostructure on the modified dielectric mask with further removal of the mask residues;

— formation of the second dielectric SiN_x mask for further formation of interdevice isolation;

— plasma-chemical etching of *n*-layers of the heterostructure on the dielectric mask to ensure the interdevice isolation;

— formation of an ohmic contact to the *n*-InP-layer of the heterostructure on the basis of the thin-film Ni/Ge/Au composition;

— planarization of the plate surface with a benzocyclobutene layer;

— formation of an ohmic contact to the *p*-InGaAs-layer of the heterostructure on the basis of the thin-film Ti/Pt/Au composition;

— formation of thin-film NiCr resistors;

— formation of interdevice bonding on the basis of Ti/Au;

— substrate separation into crystals by disc-cutting and splitting.

Modulator topology was formed using the projection *i*-line-lithography method. Optical waveguide components and interdevice isolation were formed by the reactive ion etching method using $\mathrm{Cl_2/Ar/N_2}$ gas mixture (10/20/20 $\mathrm{cm^3/min}$). For the etching process, inductive discharge power, bias power and process pressure were equal to 400 W, 90 W and 15 mTorr, respectively. Before each etching process, the carrier with substrate were cooled to room temperature (21°C). To remove etching contamination from the substrate surface, cleaning in deionized water was carried out during 2 min after etching.

Plasma-chemical etching of the heterostructure layers was performed through a single-layer SiN_x mask. SiN_x film $0.6-0.8\,\mu$m in thickness was produced on the plate surface by the plasma-chemical vapor-phase deposition method. After the lithography, the dielectric mask component topology was formed by $\mathrm{SF_6}$ reactive ion-assisted plasma etching.

Substrate surface planarization was performed using a photosensitive benzocyclobutene film, in addition, the SiN_x film was used as an adhesive sublayer. After lithography and baking operations, excessive thickness of the benzocyclobutene film was removed by the reactive ion etching method in the inductively coupled plasma using the $\mathrm{SF_6/O_2}$ gas mixture.

The ohmic contacts to the heterostructure layers, sublayer for formation of the interdevice bonding, and NiCr- thin-film resistors were formed by electron beam vacuum evaporation. Thin-film Ti/Pt/Au (50/25/400 nm) and Ni/Ge/Au (10/30/200 nm) compositions were used for bonding of ohmic contacts to *p*-InGaAs- and *n*-InP-layers of the heterostructures. The ohmic contacts were annealed on a hot plate in nitrogen atmosphere. Interdevice bonding was formed by electrochemical deposition of the $3\,\mu$m Au layer. A double-layer Ti/Au (30/80 nm) composition was used as a sublayer for deposition.

The substrate was separated into crystals by disc-cutting and splitting. Antireflection coating was not applied on the crystal ends.

Electrooptical path components of the modulator were simulated in Photon Design.

After manufacturing, modulator parametrization was performed on the optical bench. PPCL550 semiconductor laser tunable within 1530−1560 nm was used as an optical emission source. To control optical power at the modulator output, the low-frequency measurements used PM20CH

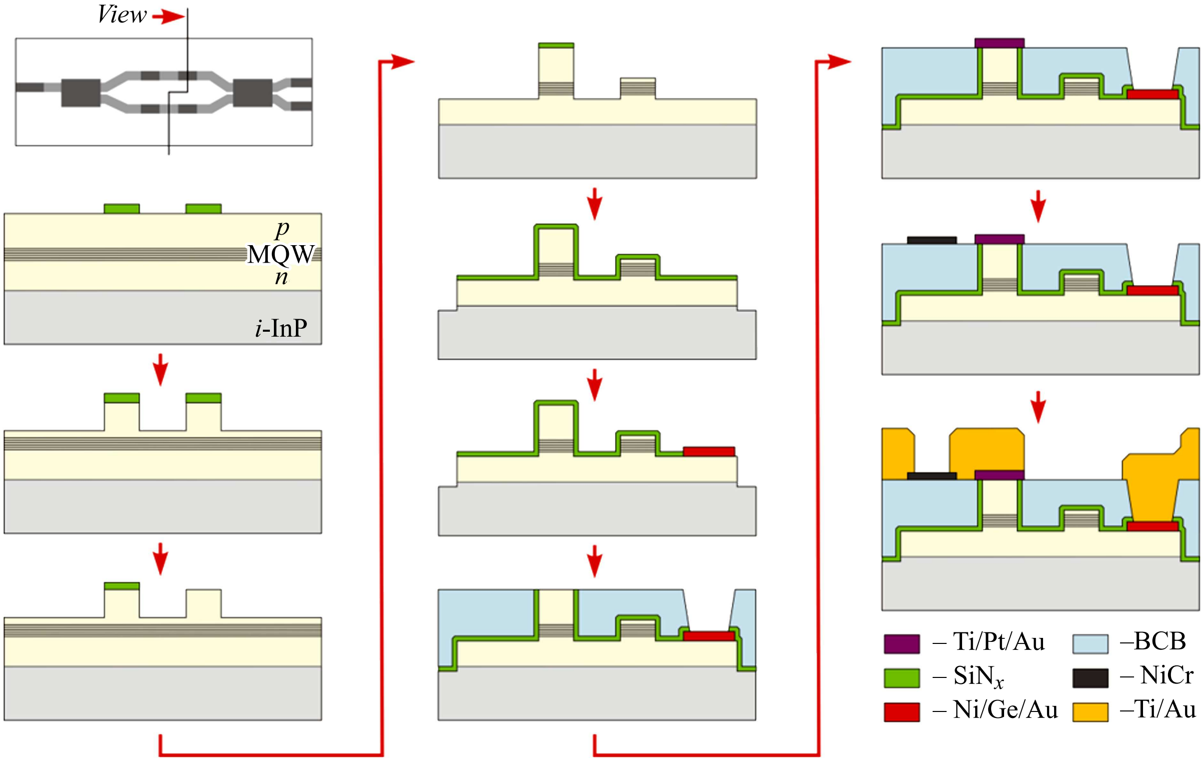

Figure 1. Manufacturing process route for InP-based Mach-Zender electrooptic modulato.

optical power meter. VHF measurements were performed using MS46122B vector circuit analyzer, and MN4765B calibration module was used as a photodetector. For optical emission input and output on the test modulators, SMF28 lens fiber was used.

2. Findings and discussion

Figure 2 shows the calculation of the maximum achievable extinction ratio of Mach-Zender EOM vs. optical power division asymmetry in the input splitter. The calculation was carried out on the assumption that no additional distortions were introduced in the interferometer arms and output optical combiner of the modulator. In practice, in most cases occasionally added manufacturing defects and design errors may additionally reduce the optical emission modulation performance. As shown in the figure, modulator ER equal to 10 dB is achieved by imbalance at the splitter output lower than 0.9 dB. This is not a record-breaking value, in commercially available modulators, ER in low-frequency measurements is usually set to 20 dB or higher [18–22]. And this value is ensured by the input splitter imbalance set lower than 0.09 dB. Higher ER values impose much stricter requirements both for design and for manufacturing process of EOM electrooptical path components in whole and of the input splitter in particular.

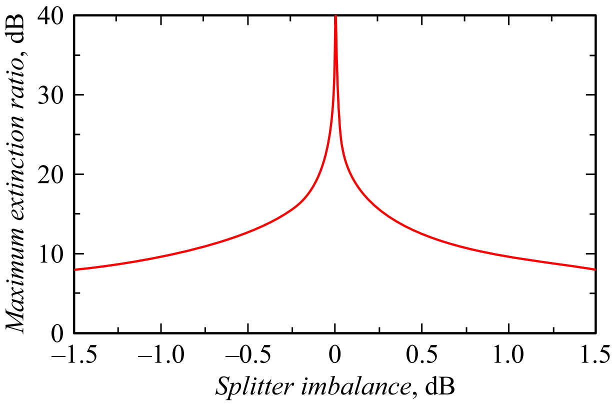

Figure 2. Calculated dependence of the EOM maximum achievable extinction ratio on the power imbalance at the beam splitter outputs at the modulator input.

The study used asymmetrical MMI (1×2) splitter as an input beam splitter. Selection of such configuration is explained by the objective of the normally off-state-modulator development. MMI (2×2) was used as an optical combiner at the EOM output. In this case, the normally off-state-state is achieved at the phase difference equal to 90° at the MMI (2×2) combiner inputs. The asymmetrical input MMI (1×2) splitter, in turn, provides the initial optical wave phase difference equal to 90° at its outputs to simplify control and reduce the EOM length. Selection of the splitter component dimensions is based, on the one hand, on minimization of sizes and optical loss in he splitter, and, on the other hand, on the process constraints. Figure 3 shows the splitter model visualization, the model

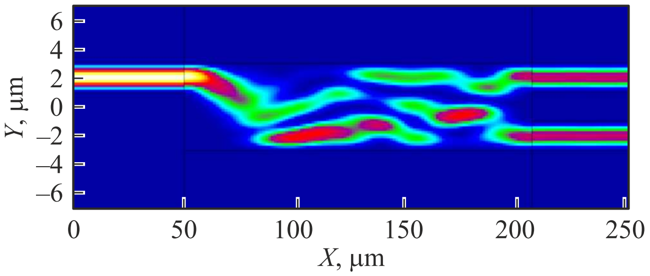

Figure 3. Visualization of the MMI (1×2) splitter model.

Table 1. MMI (1×2) splitter model parameters

Parameter	Value
Effective refraction index, n_{eff}	3.273
Width, μm	5.99
Length, μm	156
Input bias from the centerline, μm	2
Output bias from the centerline, μm	2
Division ratio	48.9:51

parameters are shown in Table 1. At the set parameters, the design optical power division ratio at the splitter outputs was equal to 48.9 : 51.

Since the splitter body length is by orders of magnitude greater than its width, the splitter body length variation in relative values will be by orders of magnitude lower at the same absolute values of process drift of its dimensions. Therefore the splitter body length variation will have much lower impact on the fringe pattern variation in MMI and the corresponding division ratio variation. Such positions of the input and output splitter waveguides are fixed at the photomask manufacturing stage. Therefore, reproduction of the splitter body width is the most critical of the splitter dimensions for manufacturing of the optical waveguide structures of the modulator.

Figure 4, *a* shows the calculated dependences of the relative optical wave power values at the outputs of the developed MMI (1×2) splitter model on the process drift of the splitter body width. Figure 4, *b* shows the corresponding maximum achievable extinction ratios in the modulator. The dependences show that the modulator extinction ratio is limited by 10 dB even when the process drift of the splitter body width is 80−90 nm. This imposes sufficiently strict requirements for the splitter manufacturing process. In addition, the process drift of the width from the optimum value causes additional reduction of the total power at the splitter outputs. But in this case, the process requirements are much softer, loss of 10% of optical wave power occurs at the splitter body width drift by at least 200−250 nm.

MMI splitter division ratio depends on the component dimensions and on the refraction index of the medium in which the optical wave propagates. When the splitter dimensions are fixed at the component manufacture stage and may not be used for dynamic control of the division ratio, then the refraction index of the medium may vary when external impacts (electric field, heating, etc.) are applied to the heterostructure. Figure 5 a shows the calculated dependence of the relative optical wave power values at he outputs of the developed MMI (1×2) splitter model on the medium refraction index variation. Figure 5, *b* shows the corresponding variation of the maximum achievable extinction ratio in the modulator. The dependences show that the refraction index variation within (−0.004) – (+0.004) ensured dynamical variation of the modulator extinction ratio in a wide range.

Figure 6 shows microscopy image of the produced modulators. The given modulator has a push-pull design. The MMI (1×2) splitter shown above was used as an input beam splitter. Phase-shifting section of the modulator is divided into the primary high-frequency half and secondary low-frequency half. At the output, the high-frequency half is loaded to a thin-film resistor (50 Ω) mounted on the modulator crystal using the monolithic technology. The secondary low-frequency half of the phase-shifting section are designed to set the modulator work point and consists of solid electrodes. Microstrip lines in both halves are loaded

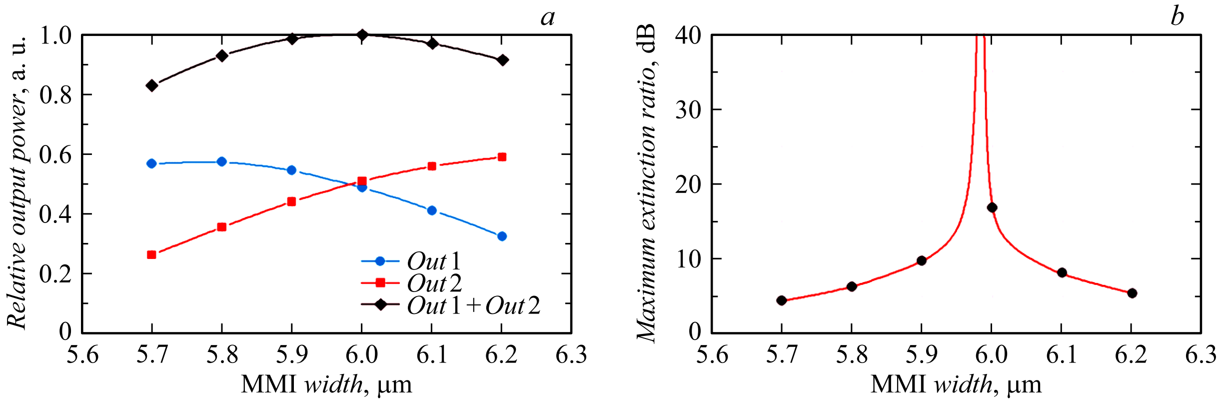

Figure 4. Calculated dependences (*a*) of the specified optical power at the MMI (1×2) splitter model outputs and (*b*) maximum achievable extinction ratio of EOM on the MMI (1×2) splitter body width at the fixed length of 156 μm.

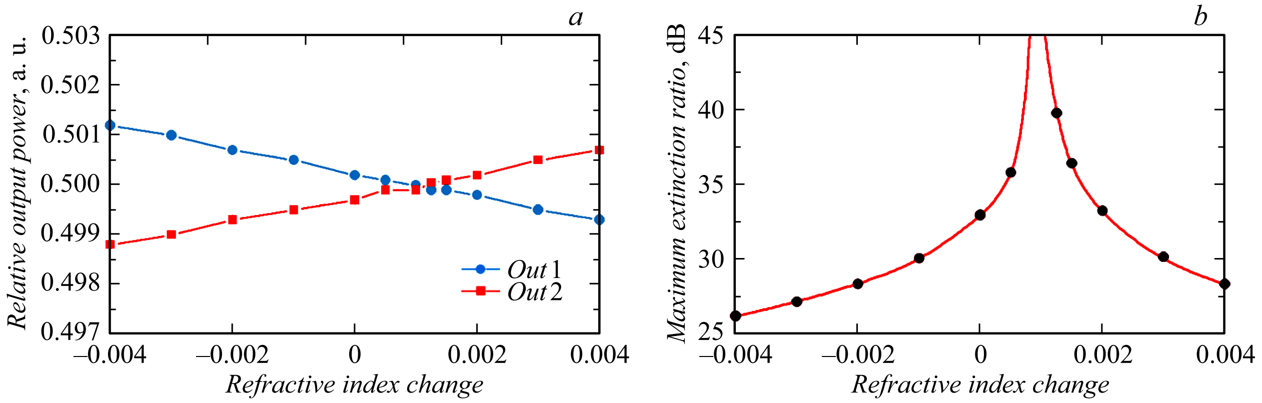

Figure 5. Calculated dependences (*a*) of the specified optical power at the MMI (1×2) splitter model outputs and (*b*) maximum achievable extinction ratio of EOM on the MMI (1×2) splitter body width at the fixed length of 5.99×156 μm.

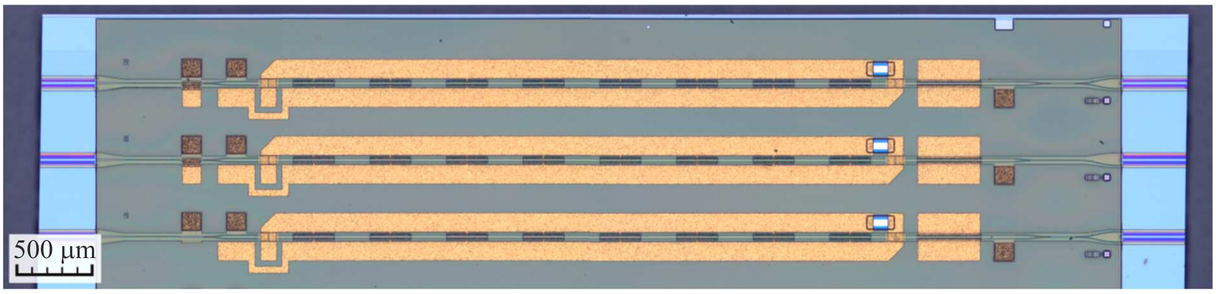

Figure 6. Microscopy image of the produced Mach-Zender EOM module.

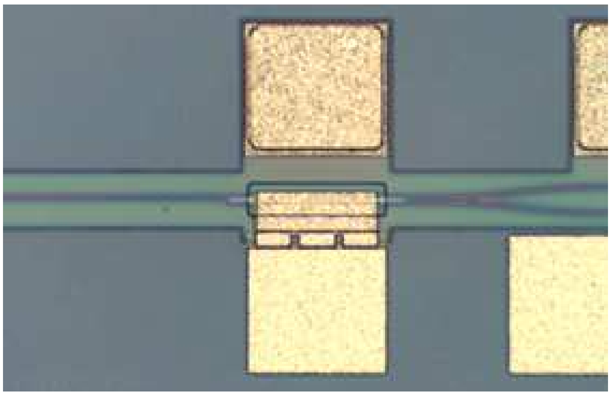

Figure 7. Microscopy image of the MMI (1×2) splitter with the fine tuning electrodes.

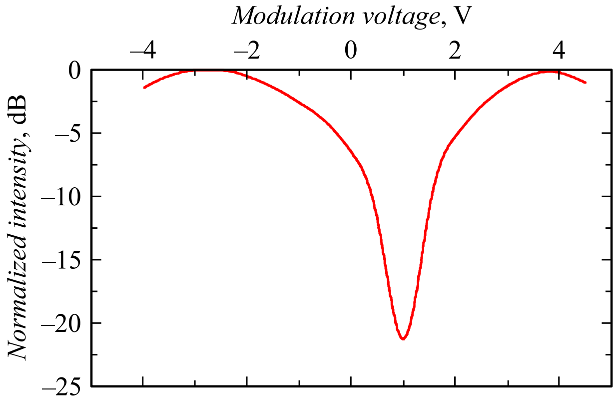

Figure 8. Measurements of the EOM optical transfer function at the bias voltage of -1 V at 1550 nm.

to *p-i-n*-diodes that simultaneously serve as the optical waveguide sections of the modulator. The MMI (2×2) combiner designed similarly to the input splitter was placed at the modulator output.

Figure 7 shows a microscopy image of the MMI (1×2) splitter placed at the modulator input. It was combined with the*p-i-n*diode to ensure control of the refraction index in the splitter's optical medium.

EOM parametrization was first performed without tuning of the input splitter division ratio. Figure 8 shows the measurements of the modulator transfer function at the bias electrode voltage of -1 V and input optical emission wavelength of 1550 nm. Modulator half-wave voltage was equal to 2.8 V, ER achieved 21.5 dB. The added loss of the modulator was equal to 6.8–7.9 dB without considering the optical wave input/output loss.

VHF measurements are shown in Figure 9. Electrooptical bandwidth of the modulator by–3 dB exceeded 32 GHz. And the modulator demonstrated good agreement of the electric signal throughout the measurement range. The

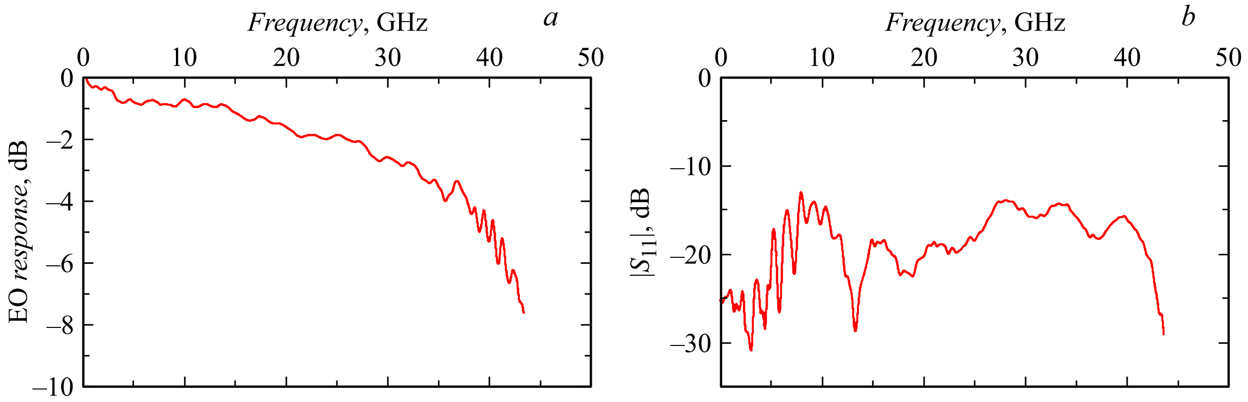

Figure 9. Measurements (a) of the electrooptical bandwidth of EOM and (b) modulus of the electric signal reflectance from the modulator input at the bias voltage of -1 V at 1550 nm.

Table 2. MMI (1×2) splitter model parameters

Reference	Year	Wavelength, nm	$f_{3\text{dB}}$, GHz	KE (LF), dB	KE (HF), dB	V_π, V	Loss, dB	length, mm
[18][1]	–	1550	35	> 20	> 10 per56 Gbaud	2.5	–	–
[23]	–	1310	58	> 20	–	3.5	4	5.5
[24]	2019	1550	31	20	–	3	2	2
[25]	2015	2000	< 9	9	–	3.2	–	6.5
[26]	2016	1550	> 67	27	> 10 per100 Gbit/s	2	2	–
[27]	2022	1550	45	> 25	5.9 per80 Gbit/s	3	–	–
[28]	2016	1550	44	25	–	2	6	–
This study	2022	1550	32	21.5–29.5 variable	–	2.8	6.8–7.9	7.4

Note. [1] Measurements in modulus.

modulus of electric signal reflectance from the input was not higher than -12 dB.

Finally, modulator ER was measured at various bias voltages on the fine tuning electrodes of the input MMI (1×2) splitter. The measurements are shown in Figure 10. They show that no significant variation of the ER modulator is observed when negative bias is applied to the *p-i-n*-structure of the splitter. It decreased slightly from initial 21.5 dB to 20.7 dB when the bias voltage of -6 V had been achieved. On the contrary, when forward bias was applied, much more pronounced dependence was observed. At the forward bias of 3 V, the modulator ER increased up to 29.5 dB.

To explain the derived dependence, the forward and reverse bias application regions shall be separated, because quite different patterns were observed in them. When reverse bias was applied to the *p-i-n*-structure, carrier concentration in MQW is low and the refraction index in the MMI splitter body is mainly measured by means of the quantum-confined Stark effect. Since the reverse voltage application did not result in considerable modulator ER variation, it was apparent that the refraction index variations were minor here. The current MMI body length is insufficient to cause significant fringe pattern variation at the MMI output and division ratio variation. manyfold increase in the MMI body length will probably causes considerable increase in the sensitivity of the division ratio increase due to the quantum-confined Stark effect and, accordingly, will ensure control of the modulator extinction ratio in a wide range.

When the forward bias is applied to the *p-i-n*-structyre, the carrier concentration in MQW increases exponentially. Here, besides the quantum-confined Stark effect, effects associated with the charge carrier injection and thermo-optical effect are enabled. In total, they have higher effect on the refraction index variation, which ensured considerable increase in the modulator ER. Like for the reverse bias, the manyfold increase in the MMI length could probably expand the adjustment range of the modulator extinction ratio or decrease the required control signal power.

Table 2 show the comparison of the developed modulator parameters with the findings of the recent studies. For the

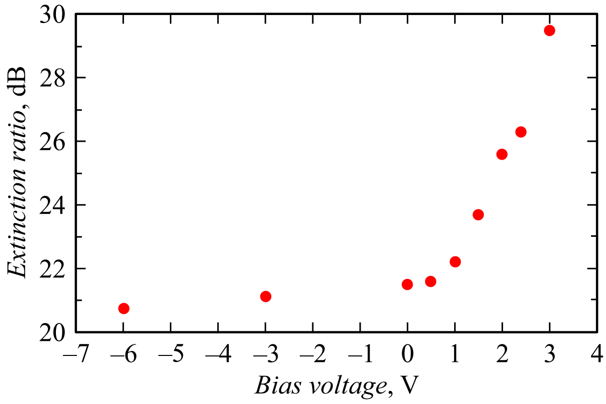

Figure 10. Dependence of the EOM extinction ratio on the bias voltage at the input MMI (1×2) splitter at 1550 nm.

main part of the parameters, the modulator shows mean values. Relatively high added loss may be reduced by optimization of the modulator topology (by decreasing its length).

Conclusion

The paper describes the results of development of the InP-based Mach-Zender electrooptic modulator with adjustable extinction ratio. Control was provided by means of electrical tuning of the division ratio of the input MMI splitter. Electrooptical bandwidth of the modulators (by −3 dB) was higher than 32 GHz, modulus of electric signal reflectance from the input was not higher than −12 dB within the range up to 43 GHz, and the half-wave voltage was equal to 2.8 V at 1550 nm. However, electrical tuning of the input splitter extended the extinction ratio of the modulator from the initial 21.5 to 29.5 dB. The adjustment range may be extended considerably by improving the input MMI splitter design. Dynamic extension of the extinction ratio may be used in practice to improve the modulator specifications as well as to simplify the manufacturing process in order reduce the final cost of products.

Funding

The study was supported financially by the Ministry of Science and Higher Education of the Russian Federation (project: Theoretical and experimental investigations of ultra-wideband optoelectronic devices of fiber optic information systems and VHF photonics on the basis of the proprietary photon integrated circuits, agreement № 075-03-2020-237/1 as of 05.03.2020, internal project No. FEWM-2020-0040).

Conflict of interest

The authors declare that they have no conflict of interest.

References

[1] Electronic media: „Cisco Annual Internet Report“ https://www.cisco.com/c/en/us/solutions/collateral/executive-perspectives/annual-internet-report/white-paper-c11-741490.html

[2] Electronic media: „NOKIA Who will satisfy the desire to consume?“ https://www.iot.gen.tr/wp-content/uploads/2017/03/160531-Nokia_Bell_Labs_Mobility_Traffic_Report.pdf

[3] M. Smit, K. Williams. J. Tol. APL Photon., **4** (5), 050901 (2019). DOI: 10.1063/1.5087862

[4] M. Smit, X. Leijtens, H. Ambrosius, E. Bente, J. Tol, B. Smalbrugge, T. Vries, E.J. Geluk, J. Bolk, R. Veldhoven, L. Augustin, P. Thijs, D. D'Agostino, H. Rabbani, K. Lawniczuk, S. Stopinski, S. Tahvili, A. Corradi, E. Kleijn, D. Dzibrou, M. Felicetti, E. Bitincka, V. Moskalenko, J. Zhao, R. Santos, G. Gilardi, W. Yao, K. Williams, P. Stabile, P. Kuindersma, J. Pello, S. Bhat, Y. Jiao, D. Heiss, G. Roelkens, M. Wale, P. Firth, F. Soares, N. Grote, M. Schell, H. Debregeas, M. Achouche, J.-L. Gentner, A. Bakker, T. Korthorst, D. Gallagher, A. Dabbs, A. Melloni, F. Morichetti, D. Melati, A. Wonfor, R. Penty, R. Broeke, B. Musk, D. Robbins. Semicond. Sci. Technol., **29** (8), 083001 (2014). DOI: 10.1088/0268-1242/29/8/083001

[5] F.M. Soares, M. Baier, T. Gaertner, N. Grote, M. Moehrle, T. Beckerwerth, P. Runge, M. Schell. Appl. Sci., **9** (8), 1588 (2019). DOI: 10.3390/app9081588

[6] Electronic media: „1550 nm DFB Laser Diode, PM Output, High Performance. Data Sheet.“ https://lenlasers.ru/upload/iblock/b31/DFB_1550_PM_HP.LLS.pdf

[7] Electronic media: „DFB & DBR Laser Diodes. DFB stock list.“ https://www.toptica.com/fileadmin/Editors_English/14_stocklists/DFB-Stock-list.pdf

[8] Electronic media: „1550 nm laser diode — DFB. Data Sheet.“ https://www.aerodiode.com/wp-content/uploads/2020/05/1550-nm-laser-diode-Model-1-Datasheet-4.pdf

[9] L.B. Soldano, E.C.M. Pennings. J. Lightwave Technol., **13** (4), 615 (1995). DOI: 10.1109/50.372474.

[10] J. Leuthold, C.H. Joyner. J. Lightwave Technol., **19** (5), 700 (2001). DOI: 10.1109/50.923483

[11] D.A. May-Arrioja, P. LiKamWa, C. Velasquez-Ordonez, J.J. Sanchez-Mondragon. Electron. Lett., **43** (13), 714 (2007). DOI: 10.1049/el:20071070

[12] D.A. May-Arrioja, P. LiKamWa, J.J. Sanchez-Mondragon, R.J. Selvas-Aguilar, I. Torres-Gomez. Meas. Sci. Technol., **18** (10), 3241 (2007). DOI: 10.1088/0957-0233/18/10/S29

[13] J. Klamkin, L.A. Johansson, A. Ramaswamy, H.F. Chou, M.N. Sysak, J.W. Raring, N. Parthasarathy, S.P. DenBaars, J.E. Bowers, L.A. Coldren. In: 2006 *Conf. on Optoelectronic and Microelectronic Materials and Devices* (Perth, Australia, 2006), p. 184. DOI: 10.1109/COMMAD.2006.4429911

[14] J. Klamkin, A. Ramaswamy, L.A. Johansson, N. Nunoya, J.E. Bowers, S.P. DenBaars, L.A. Coldren. In: 2009 *International Topical Meeting on Microwave Photonics* (Valencia, Spain, 2009), https://coldren.ece.ucsb.edu/sites/default/files/publications/klamkin_-_uni-traveling-carrier_balanced_photodiode.pdf

[15] H.G. Bukkems, R.C. Strijbos, J.J.M. Binsma, H. Vrieze, M.C. Larson, M.K. Smit, E.A.J.M. Bente, B.H. Verbeek. J. Quantum Electron., **43** (7), 614 (2007). DOI: 10.1109/JQE.2007.899406

[16] D.A. May-Arrioja, P. LiKamWa, R.J. Selvas-Aguilar, J.J. Sanchez-Mondragon. Opt. Quant. Electron., **36** (15) 1275 (2004). DOI: 10.1007/s11082-005-0317-2

[17] B. Mao, P. Yue, F. Hou, Z. Liu. J. Eur. Opt. Soc.-Rapid., **10**, 15004 (2015). DOI: 10.2971/jeos.2015.15004

[18] Electronic media: „C-band 56GBaud InP Mach-Zehnder-Modulator. Data sheet." https://www.hhi.fraunhofer.de/fileadmin/PDF/PC/MOD/datasheet_module_MZM_1550_56Gbaud_TECincl_v2.pdf

[19] Electronic media: „Lithium Niobate Electro-Optic Modulators, Fiber-Coupled (1260 nm−1625 nm). Specifications." https://www.thorlabs.com/newgrouppage9.cfm?objectgroup_id=3918

[20] Electronic media: „Lithium Niobate Electro Optic Modulator. Specifications." https://www.ixblue.com/photonics-space/intensity-modulators/

[21] Electronic media: „40G Intensity Modulator Sumitomo T.MXH1.5-40PD-ADC." http://www.hltoptical.com/page420?product_id=249&_l=en

[22] Electronic media: „100G IQ-QAM Modulator Oclaro PM100."http://www.hltoptical.com/page420?product_id=337&_l=en

[23] Electronic media: „O-band 100GBaud InP Mach-Zehnder-Modulator. Data sheet." https://www.hhi.fraunhofer.de/fileadmin/PDF/PC/MOD/datasheet_chip_MZM_1300_100Gbaud_v2.pdf

[24] G. Qian, B. Niu, W. Zhao, Q. Kan, X. Gu, F. Zhou, Y. Kong, T. Chen. Chin. Opt. Lett., **17** (6), 061301 (2019). DOI: 10.3788/COL201917.061301

[25] M.U. Sadiq, M.R. Gleeson, N. Ye, J. O'Callaghan, P. Morrissey, H.Y. Zhang, K. Thomas, A. Gocalinska, E. Pelucchi, F.C.G. Gunning, B. Roycroft, F.H. Peters, B. Corbett. Opt. Express, **23** (9), 10905 (2015). DOI: 10.1364/OE.23.010905

[26] Y. Ogiso, J. Ozaki, N. Kashio, N. Kikuchi, H. Tanobe, Y. Ohiso, M. Kohtoku. Electron. Lett., **52** (22), 1866 (2016). DOI: 10.1049/el.2016.2987

[27] Y.D. Gupta, G. Binet, W. Diels, J.A. Heibach, J. Hogan, M. Baier, M. Schell. In: 2022 *European Conference on Optical Communication* (Basel, Switzerland, 2022), https://ict-poetics.eu/wp-content/uploads/2022/07/MZMs_ECOC_2022_v1-ydg-10052022.pdf

[28] S. Lange, M. Gruner, C. Meuer, R. Kaiser, M. Hamacher, K.-O. Velthaus, M. Schell. J. Light. Technol., **34** (2), 401 (2016). DOI: 10.1109/JLT.2015.2496426

Translated by Ego Translating